

# Doping effect investigation of Li-doped nanostructured ZnO thin films prepared by sol–gel process

F. Boudjouan<sup>1</sup> · A. Chelouche<sup>1</sup> · T. Touam<sup>2</sup> · D. Djouadi<sup>1</sup> · R. Mahiou<sup>3</sup> · G. Chadeyron<sup>3</sup> · A. Fischer<sup>4</sup> · A. Boudrioua<sup>4</sup>

Received: 3 February 2016 / Accepted: 7 April 2016 / Published online: 13 April 2016  
© Springer Science+Business Media New York 2016

**Abstract** In this work, we report the effects of Li doping concentration (5, 10 and 15 at.%) on structural, morphological, electrical and optical properties of Li doped ZnO films. We used X-ray diffraction (XRD), scanning electronic microscopy (SEM), Hall-Effect measurements, UV–Vis–NIR and photoluminescence (PL) spectroscopies. XRD patterns showed that the deposited films had a hexagonal-wurtzite crystal structure with preferred orientation along the *c*-axis. SEM micrographs indicated that grain dispersion in the films were homogeneous. Hall-effect measurements revealed that ZnO thin films doped with 5, 10 and 15 at.% of Li have *p*-type conduction. The UV–Vis–NIR spectroscopy analyses demonstrated that all thin films were highly transparent in the visible region and the optical transmittance was dependent on the Li doping content. Room temperature PL spectra put into evidence that all Li-doped ZnO thin films emitted a UV-blue light and the emission intensities were found to be affected by Li concentration.

## 1 Introduction

In recent years, ZnO has been largely investigated due to its interesting properties, such as, wide and direct band gap (3.37 eV at room temperature), large exciton binding energy (60 meV), high refractive index and piezoelectricity [1–3]. These attractive properties opened up, for ZnO, a wide range of applications such as UV light emitting diodes and laser diodes [4, 5], gas sensors [6], optical waveguide [2, 7] and solar cells [8]. However, the doping of this material to obtain *n*-type and *p*-type is necessary for the development of optoelectronics ZnO based devices. It is well known that naturally ZnO presents *n*-type conduction due to zinc interstitials or oxygen vacancies native defects. Nevertheless, the achievement of stable *p*-type ZnO is difficult due mainly to self-compensation of acceptors by native defects [9, 10]. The presence of residual impurities in significant concentrations of donor type is another problem limiting *p*-type conduction in ZnO [11].

It was demonstrated [12] that *p*-type ZnO can be substitutionally achieved by the incorporation of Li atoms on Zn-sites (formation of Li<sub>Zn</sub> acceptors). However, Li is known to be very mobile in the ZnO-lattice due to its small ionic radius, which can lead to the formation of interstitial (Li<sub>i</sub>) defects acting as donors [12, 13]. Therefore, the formation of Li<sub>i</sub> defects is responsible of the frequent observation of semi-insulating behavior of ZnO: Li material and the significant control of Li incorporation on the Zn-lattice site [14].

Up till now, few reports have been published on *p*-type Li-doped ZnO thin films using various methods [15–22] and concerning the investigation of preparation conditions such as post annealing temperature and Li doping concentration on thin film electrical properties. However, to

---

✉ A. Chelouche  
azeddinechelouche@gmail.com

<sup>1</sup> Laboratoire de Génie de l'Environnement, Université de Bejaia, 06000 Bejaia, Algeria

<sup>2</sup> Laboratoire des Semi-conducteurs, Université Badji Mokhtar-Annaba, 23000 Annaba, Algeria

<sup>3</sup> Université Clermont Auvergne, Institut de Chimie de Clermont-Ferrand, UMR 6296 CNRS/UBP/Sigma Clermont, 63171 Aubière, France

<sup>4</sup> Laboratoire de Physique des Lasers, Université Paris, 13, Sorbonne Paris Cité, 93430 Villetaneuse, France

the best of our knowledge, there has been only a couple of published works on sol–gel Li-doped ZnO *p*-type nanostructured thin films [21, 22]. It was pointed out that the *p*-type conduction can be achieved for Li concentration greater than or equal to 10 at. %.

In this work, undoped and Li-doped ZnO thin films were deposited on glass substrates using a sol–gel dip-coating process and lithium acetate as doping source. The effects of Li content on the structural, morphological, optical and electrical properties of sol–gel Li-doped ZnO (ZnO:Li) nanostructured thin films was investigated by using different characterization techniques.

## 2 Experiments

### 2.1 Preparation conditions

Sol–gel process was used to prepare ZnO films. As a starting material, zinc acetate dehydrate ( $\text{Zn}(\text{CH}_3\text{COO})_2 \cdot 2\text{H}_2\text{O}$ ) (sigma Aldrich) was dissolved in a mixture of pure ethanol and monoethanolamine (MEA,  $\text{C}_2\text{H}_7\text{NO}$ ). Lithium acetate were added to zinc acetate to obtain sols with 5, 10, and 15 at. % concentrations. The MEA to Zn ratios was kept at 1.0 [23]. The final concentration of zinc acetate in the solution was kept at 0.4 M. All prepared ZnO sols were maintained under continuous magnetic stirring at 50 °C for 1 h. Glass substrates were washed with a liquid detergent, rinsed with distilled water, and then immersed in 4 M nitric acid for 24 h. They were then ultrasonically cleaned and rinsed in ethanol and distilled water during 15 min at 60 °C and, finally, were dried at 100 °C for 2 h. The deposition was carried out using a KSV dip-coater with a withdrawal speed of 1.5 cm/min and the number of deposited layers on the glass substrates was set to six. The deposited films were preheated at 200 °C for 15 min after each coating. The films were subsequently heated up to 500 °C for 1 h in order to obtain crystallized ZnO.

### 2.2 Characterization techniques

The crystalline structure of ZnO thin films was characterized with a PanAlytical X-ray diffractometer using Cu  $K\alpha$  radiation and operating at an accelerating voltage of 40 kV and an emission current of 30 mA. Micro-structures of the deposited films were analyzed by the SEM technique using a Raith PIONEER System. The Hall Effect measurement was carried out to investigate the *n*-type or *p*-type nature of the films and to estimate their carrier concentration, resistivity and carrier mobility. The measurement was performed at Room temperature in the Van der Pauw configuration using an HMS-3000 Ecopia Hall-effect measurement system. The optical transmittance spectra

were recorded at room temperature by a Safas UVmc<sup>2</sup> UV–Visible spectrophotometer. The measurements were taken at a normal incidence with respect to air. The optical band gap energy data was then derived from the transmission spectra. The photoluminescence properties were measured at room temperature using Xenon lamp operating at 350 nm. The incident beam was focused perpendicularly to the film surface and the fluorescence was collected in a guiding mode using a TRIAX 550 Horiba–Jobin Yvon monochromator equipped with a nitrogen cooled CCD camera.

## 3 Results and discussion

### 3.1 Structural and morphological properties

Figure 1 shows XRD patterns of undoped and Li-doped ZnO thin films at different Li concentrations (5, 10 and 15 at. %). These patterns reveal that all the investigated films exhibit only the (002) peak of the ZnO hexagonal wurtzite structure (JCPDS card N°:36-1451). However, a very weak (101) ZnO peak was also observed in undoped ZnO film pattern. The patterns clearly demonstrate that all the films are highly oriented along *c*-axis direction. This result is the consequence of the self-ordering effect caused by the minimization of ZnO crystal surface free energy. It can also be noted that there is no signature of extra secondary phases related to Li compounds even at higher Li content indicating that doping with Li does not alter the ZnO crystalline structure. Furthermore, the (002) peak intensity increases with increasing Li doping level up to 10 at. %, then decreases for higher concentration. The enhancement of crystal quality at low doping concentrations may be attributed to the formation of new nucleating centers due to dopant atoms resulting from the decrease of nucleation energy barrier [24, 25]. However, the decrease

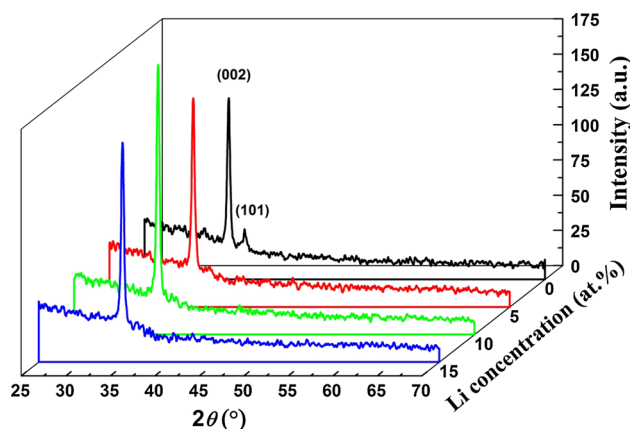


**Fig. 1** XRD patterns of undoped and Li-doped ZnO thin films

of the intensity of (002) peak for the Li-doped ZnO at 15 at.% may be due to the increase of the occupation of  $\text{Li}^+$  ion in the interstitial position rather than substitution of  $\text{Zn}^{2+}$  site and eventually to the segregation of Li at the grain boundary [26].

The crystallite size, lattice parameters and  $c/a$  ratio calculated from Rietveld refinement using MAUD analysis software program, are summarized in Table 1. The results show that Li concentration lower than 10 at.% does not significantly affect the crystallite size while doping with Li content greater than 10 at.% causes the increase of crystallite size as better illustrated in Fig. 2. This behavior may be due to the increase of imperfections such as point defects and dislocations, which enhance grain boundary mobility and growth rate [27]. Furthermore, the  $c/a$  ratio seems to be affected by Li content. In fact, this ratio decreases with increasing Li concentration up to a minimum value of 1.6003 for the ZnO thin film doped at 10 at.% and then increases for the ZnO film doped at 15 at.%. It should be noted that it is largely accepted in literature that in doped ZnO crystals, the wurtzite structure deviates from the ideal arrangement by changing  $c/a$  ratio [28]. This change is mainly due to the difference in the electronegativity between the two component elements: deviation from the ideal  $c/a$  ratio is more important for components with larger electronegativity differences ( $\text{Li} = 0.98$ ;  $\text{Zn} = 1.65$ ). Based on the work reported by Morkoç and Özgür [28], we can deduce that the greatest difference in electronegativity is recorded for the sample doped at 10 at.% suggesting higher  $\text{Li}_{\text{Zn}}$  acceptor defects density. Since the electronegativity of the oxygen is 3.44, the electronegativity difference between Zn and O atoms is 1.79. However, in the case of the Zn atom is replaced by Li, the difference in electronegativity becomes 2.46. Further increase in  $c/a$  ratio for Li-doped ZnO at 15 at.% may be due to the decrease of electronegativity difference in the sample indicating a possible incorporation of  $\text{Li}_i$  donor defects which may lead to the formation of neutral  $\text{Li}_{\text{Zn}}\text{-Li}_i$  complexes. These results can be explained by the fact that smaller Li radius can easily occupy an interstitial position.

Figure 3 shows high magnification SEM images of the undoped and Li-doped ZnO thin films on glass substrates. It can be seen that grains dispersion in the films is homogeneous. However, the surface morphology of the films seems to be slightly dependent on Li doping. In particular,

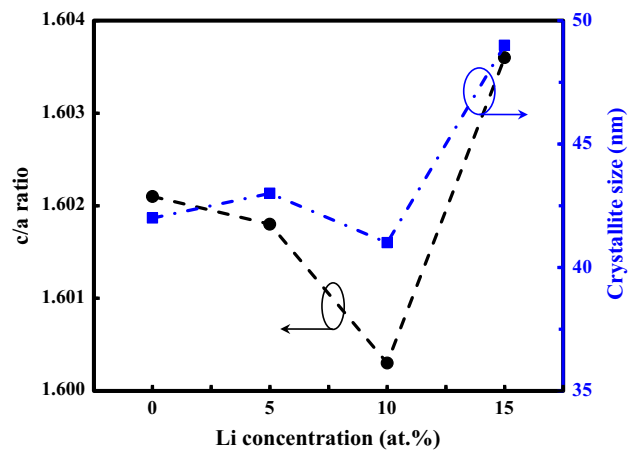


Fig. 2  $c/a$  ratio and crystallite size of Li-doped ZnO thin films

the grains size of the 15 at.% doped film is slightly larger, indicating that high Li doping concentrations promote the crystallites agglomeration. This result is in agreement with XRD analysis. Moreover, it can be seen that some pores are apparent in the undoped and 15 at.% Li-doped ZnO thin films, while denser morphology is observed for the samples doped at 5 and 10 at.%. The enhancement in the surface coverage of these two films may be attributed to the increase of the nucleation centers, which is the result of the decrease of nucleation energy barrier. However, for higher concentrations, Li atoms may segregate at the grain boundary leading to increased agglomeration of the crystallites, which, in turn, leads to larger grains with the presence of pores. These observations are in a good agreement with XRD results.

### 3.2 Electrical and optical properties

The electrical properties of undoped and Li-doped ZnO thin films were measured at room temperature using Hall-Effect measurements at Van der Pauw configuration. The measurements were repeated several times for all the samples in order to examine the reliability and repeatability of the conduction of the films. The results are summarized in Table 2. They show that electrical properties of ZnO films are dependent on Li doping content. The undoped ZnO thin film exhibits  $n$ -type conduction, whereas all the doped films present  $p$ -type behavior. It is widely accepted

**Table 1** Rietveld refined XRD data of Li-doped ZnO at various doping concentrations

Li-doping (%)	$a$ parameter (nm)	$c$ parameter (nm)	$c/a$	Crystallite size (nm)
0	0.3257	0.5218	1.6021	42
5	0.3257	0.5217	1.6018	43
10	0.3260	0.5217	1.6003	41
15	0.3254	0.5218	1.6036	49

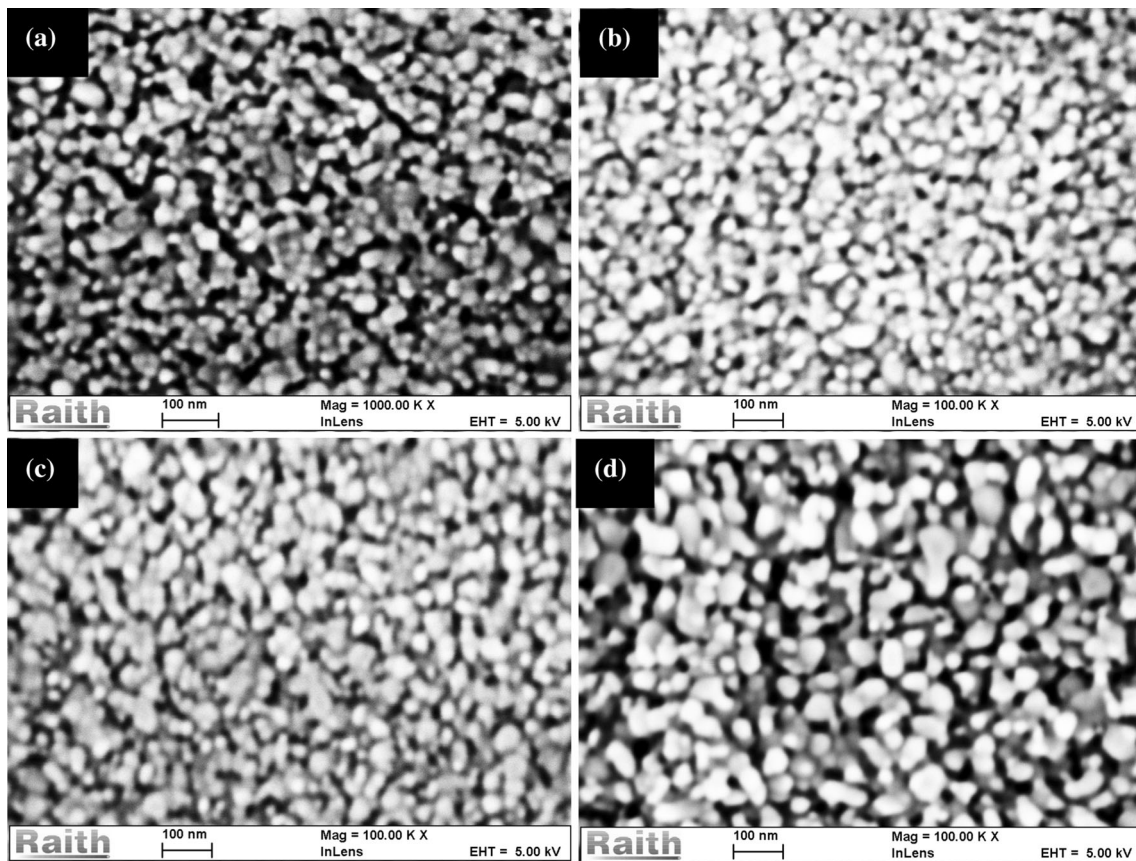


**Fig. 3** SEM micrographs of Li-doped ZnO thin films **a** Li = 0 at.%, **b** Li = 5 at.%, **c** Li = 10 at.% and **d** Li = 15 at.%

**Table 2** Electrical properties and optical band gap of Li-doped ZnO films

Li concentration (%)	Carrier concentration ( $\text{cm}^{-3}$ )	Hall mobility ( $\text{cm}^2/\text{Vs}$ )	Resistivity ( $\Omega/\text{cm}$ )	Carrier type	$E_g$ (eV)
0	$4.32 \times 10^{14}$	11.11	1299	<i>n</i>	3.229
5	$1.38 \times 10^{15}$	4.96	911	<i>p</i>	3.239
10	$9.25 \times 10^{15}$	3.16	213	<i>p</i>	3.246
15	$4.09 \times 10^{15}$	4.7	325	<i>p</i>	3.234

that the *p*-type conduction in Li-doped ZnO results from the substitution of the Zn vacancy by Li atoms ( $\text{Li}_{\text{Zn}}$ ) acting as acceptors [29]. Since the sol used for ZnO deposition was rich on oxygen (0.4 M), the undoped thin film may contain a large  $V_{\text{Zn}}$  density. Thus in O-rich medium, the probability of having formed  $\text{Li}_{\text{Zn}}$  acceptors should be very high after doping with Li atoms. Therefore, the transition from *n*-type to *p*-type in our case may be due to the occupation of Zn-vacancy ( $V_{\text{Zn}}$ ) in undoped film by substitutional Li ( $\text{Li}_{\text{Zn}}$ ) in the Li-doped samples. Moreover, the density of these acceptors could increase with increasing Li concentration up to the occupation of all  $V_{\text{Zn}}$  defects leading to the increase in the hole concentration. As can be

seen in Fig. 4, the carrier concentration increases with Li doping concentration, until it reaches a maximum value for 10 at.% Li doping and then decreases; whereas an opposite trend is observed in the films resistivity. The decrease of the film resistivity for Li doping less than 10 at.% may be attributed to the improvement of the crystalline quality and the surface coverage of the deposited films. Further increase in Li content to 15 at.% leads to a slight degradation of the crystalline quality and the deterioration of the sample surface morphology. However, as can be seen from Table 2, the carrier mobility decreases with increasing the doping which may be explained by the enhancement of the grain boundary scattering [30]. The enhancement of hole

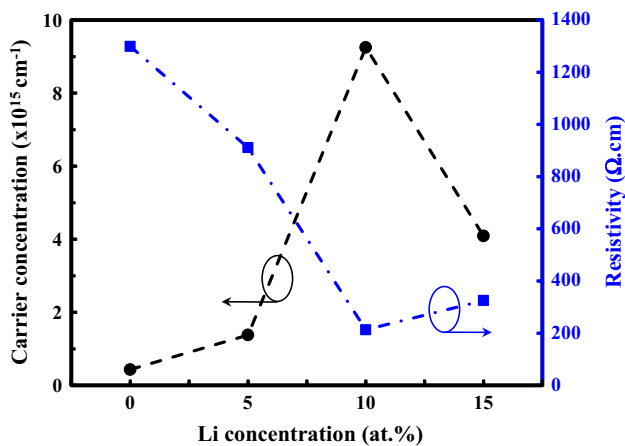


**Fig. 4** Carrier concentration and resistivity of Li-doped ZnO thin films

concentration with Li doping could be due to the increase of  $\text{Li}_{\text{Zn}}$  acceptors defects density. In addition to that, further increase in Li concentration leads to the formation of  $\text{Li}_i$  donors and possible existence of  $\text{Li}_{\text{Zn}}\text{-Li}_i$  complexes in the sample doped at 15 at.% Li. These donors act as hole traps and thus contribute to the reduction of hole concentration. Similar results have been reported by Wang et al. [21]. These results are in a very good agreement with XRD and SEM analysis.

Figure 5 displays the optical absorption spectra of undoped and Li-doped ZnO thin films at different concentrations. All deposited films present a high transparency ranging from 71 to 92 %. However, the films transmittance seems to be affected by Li contents. It can be clearly seen that the average transmittance increases with increasing Li content up to 10 at.% and then slightly decreases for the sample doped at 15 at.%. The increase in film transparency

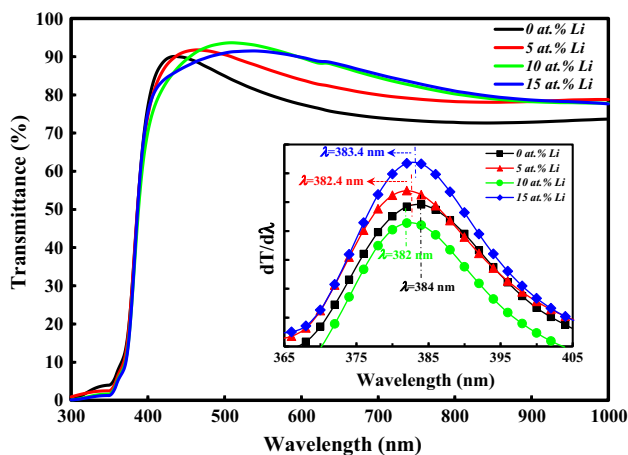


**Fig. 5** UV-Vis-NIR transmittance spectra of undoped and Li-doped ZnO thin films. *Inset* plots of the derivative of the transmittance with respect to wavelength

may be due to the improvement of crystal quality, which leads to lowering the light diffusion by grains forming the film. Similar trend has been also observed by Bagheri et al. [31] in sol-gel Li-doped ZnO films. This result confirms the XRD measurement.

The first derivative curve of the optical transmittance ( $dT/d\lambda$ ), depicted in the insert of Fig. 5, was used to estimate the energy band gap of the films, which is calculated from the following equation [32]:

$$E_g = hc/\lambda_{\text{max}}$$

where  $h$  is Planck constant,  $c$  is the light velocity and  $\lambda_{\text{max}}$  is the wavelength at which the first derivative curve gives a maximum.

The obtained optical band gap energy values are listed in Table 2. The results indicate that  $E_g$  initially increases with increasing Li doping up to 10 at.% and then decreases for higher doping concentration. This band gap behavior cannot be attributed to the quantum size effect since the crystallite size is larger than ZnO Bohr exciton radius. Consequently, the blue shift of the band gap of the films for Li concentrations less than 10 at.% can be explained by the Burstein-Moss effect. Indeed, since the Fermi level of  $p$ -type semiconductors lies in the valence band and its position depends on hole concentration, the energy required for electron excitation from this level to conduction band increases with lowering Fermi level. The position of the Fermi level is much lower when the concentration of the holes is larger. Thus, the slight decrease of the band gap of the sample doped at 15 at.% is due to the decrease of hole concentration. Similar trends have been reported in literature [33, 34]. These results are in a good agreement with Hall-Effect measurement.

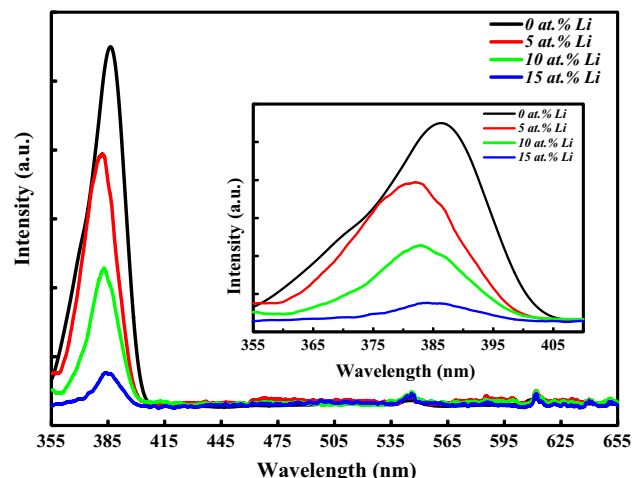


**Fig. 6** Room temperature PL spectra of undoped and Li-doped ZnO thin films. *Inset* magnification of the UV emission region

Figure 6 shows room-temperature PL spectra of ZnO:Li films with different Li doping concentrations. The insert of the Fig. 6 depicts selected UV emission. All the films present only a UV band due to the near-band-edge (NBE) emission. The absence of the visible emission indicates a high quality of the samples and the presence of small defects densities of some native defects such as oxygen vacancy and zinc interstitial in the films structures [35]. It is observed that the intensity of the UV emission decreases with the increase in Li content. Similar behavior was reported by Kumar et al. [36] who found that the intensity of the UV emission peak decreases with the increase of Na doping ZnO. It was pointed out that the increment of non-radiative recombination centers introduced by Na doping was responsible of this decrease in UV emission. Moreover, Tirpak et al. [37] have reported that the NBE emission in Sb-doped *p*-type ZnO decreases with increasing hole concentration. Based on these works, the decrease in the intensity of the UV emission with increasing Li doping up to 10 at.%, observed in our work, can be attributed to the increase of hole concentration. Whereas the further decrease of this emission of the film doped at 15 at.% Li cannot be explained by the increase of hole concentration since a slight decrease of these carrier concentrations has been found. El Ghoul et al. [38] have observed a decrease in ZnO UV emission with increasing Co doping concentration. It was pointed out that such a decrease is attributed to the deterioration of crystalline quality with Co doping. Wang et al. [39] have also ascribed the decrease in UV emission of Al doped ZnO films with increasing Al content to the degradation of the ZnO crystal quality. Thus, such a decrease of UV emission for the sample doped at 15 at.% Li may be due to the increase of non-radiative emission caused by the degradation of the crystalline quality. Moreover, the UV emission of doped ZnO thin film at Li concentrations below 10 at.% is slightly blue shifted as compared to the undoped one. Such a blue shift is attributed to the increase of the band gap as demonstrated by transmittance results.

#### 4 Conclusions

Undoped and Li-doped ZnO thin films were synthesized on glass substrates by using sol–gel dip-coating process. XRD analyses revealed that all films had a hexagonal wurtzite structure with *c*-axis orientation, and Li doping could improve the crystalline quality of the ZnO films. SEM micrographs of all the samples showed homogeneous grain distribution with a denser surface morphology observed at 10 at.% Li concentration. Hall-Effect measurements revealed that all doped films have *p*-type conductivity with hole mobility values ranging between 3 and 5 cm<sup>2</sup>/V.s.

UV–Vis–NIR transmittance spectra indicated that all films were highly transparent with average visible transmission values ranging from 71 to 92 %. Moreover, it was found that the optical band gap slightly increases with increasing Li doping up to 10 at.% and then decreases for higher doping concentration. Room temperature PL results put into evidence that all the films exhibit only a UV emission band which displays a decrease in intensity with increasing Li concentration.

**Acknowledgments** This research was supported in part by a grant from the Agence Thématique de Recherche en Sciences & Technologie (ATRST), Alger, Algeria. The authors are grateful to Mr. S. Ouhenia for his help in the calculation using MAUD analysis software program.

#### References

1. Ü. Özgür, Y.I. Alivov, C. Liu, A. Teke, M.A. Reshchikov, S. Doğan, V. Avrutin, S.-J. Cho, H. Morkoç, *J. Appl. Phys.* **98**, 041301 (2005)
2. M. Tazerout, A. Chelouche, T. Touam, D. Djouadi, F. Boudjouan, S. Khodja, S. Ouhenia, A. Fischer, A. Boudrioua, *Eur. Phys. J. Appl. Phys.* **67**, 10502 (2014)
3. A. Khan, M. Hussain, O. Nur, M. Willander, *J. Phys. D Appl. Phys.* **47**, 345102 (2014)
4. Q. Feng, J. Liu, J. Lu, Y. Mei, Z. Song, P. Tao, D. Pan, Y. Yang, M. Li, *Mater. Sci. Semicond. Proc.* **40**, 436 (2015)
5. C.Y. Liu, H.Y. Xu, Y. Sun, J.G. Ma, Y.C. Liu, *Opt. Express* **22**(14), 16731 (2014)
6. J. Jońca, A. Ryzhikov, M.L. Kahn, K. Fajerweg, B. Chaudret, A. Chapelle, P. Menini, P. Fa, *Procedia Eng.* **87**, 907 (2014)
7. S. Khodja, T. Touam, A. Chelouche, F. Boudjouan, D. Djouadi, Z. Hadjoub, A. Fischer, A. Boudrioua, *Superlattice Microst.* **75**, 485 (2014)
8. M. Giannouli, F. Spiliopoulou, *Renew. Energy* **41**, 115 (2012)
9. S. Lany, J. Osorio-Guillen, A. Zunger, *Phys. Rev. B* **75**, 241203 (2007)
10. A. Janotti, C.G. Van de Walle, *Phys. Rev. B* **76**, 165202 (2007)
11. J.-L. Santailier, C. Audoin, G. Chichignoud, R. Obrecht, B. Kaouache, P. Marotel, D. Pelenc, S. Brochen, J. Merlin, I. Bisotto, C. Granier, G. Feuillet, F. Levy, *J. Cryst. Growth* **312**, 3417 (2010)
12. X.Y. Duan, R.H. Yao, Y.J. Zhao, *Appl. Phys. A Mater. Sci.* **91**, 467 (2008)
13. D.C. Look, B. Clafin, *Phys. Stat. Sol. (b)* **241**(3), 624 (2004)
14. E.-C. Lee, K.J. Change, *Phys. Rev. B* **70**, 115210 (2004)
15. S.-Y. Tsai, M.-H. Hon, Y.-M. Lu, *J. Cryst. Growth* **326**, 85 (2011)
16. S. Ghosh, G.G. Khan, A. Ghosh, S. Varma, K. Mandal, *Cryst. Eng. Comm.* **15**, 7748 (2013)
17. Z. Zhang, K.E. Knutsen, T. Merz, A. Yu Kuznetsov, B.G. Svensson, L.J. Brillson, *J. Phys. D Appl. Phys.* **45**, 375301 (2012)
18. S. Yu, L. Ding, H. Zheng, C. Xue, L. Chen, W. Zhang, *Thin Solid Films* **540**, 146 (2013)
19. B. Xiao, Z. Ye, Y. Zhang, Y. Zeng, L. Zhu, B. Zhao, *Appl. Surf. Sci.* **253**, 895 (2006)
20. K.-H. Wu, L.-Y. Peng, M. Januar, K.-C. Chiu, K.-C. Liu, *Thin Solid Films* **570**, 417 (2014)
21. D. Wang, J. Zhou, G. Liu, *J. Alloys Compd.* **481**, 802 (2009)
22. T. Wang, M. Dai, Y. Yan, H. Zhang, Y. Yu, *Appl. Mech. Mater.* **734**, 796 (2015)

23. F. Boudjouan, A. Chelouche, T. Touam, D. Djouadi, S. Khodja, M. Tazerout, Y. Ouerdane, Z. Hadjoub, J. Lumin. **158**, 32 (2015)
24. G. Li, X. Zhu, X. Tang, W. Song, Z. Yang, J. Dai, Y. Sun, X. Pan, S. Dai, J. Alloys Compd. **509**, 4816 (2011)
25. M. Öztas, M. Bedir, Thin Solid Films **516**, 1703 (2008)
26. R. Vettumperumal, S. Kalyanaraman, B. Santoshkumar, R. Thangavel, Mater. Res. Bull. **50**, 7 (2014)
27. J.A. Najim, J.M. Rozaiq, Int. Lett. Chem. Phys. Astron. **10**(2), 137 (2013)
28. H. Morkoç, Ü. Özgür, *Zinc Oxide: Fundamentals Materials and Device Technology* (Wiley, Weinheim, 2009)
29. J.C. Fan, K.M. Sreekanth, Z. Xie, S.L. Chang, K.V. Rao, Prog. Mater. Sci. **58**, 874 (2013)
30. S.S. Shinde, C.H. Bhosale, K.Y. Rajpure, J. Photochem. Photobiol. B **120**, 1 (2013)
31. N. Bagheri, M.M. Ara, N. Ghazyani, J. Mater. Sci.: Mater. Electron. **27**, 1293 (2016)
32. N. Veissid, C.Y. An, A. Ferreira da Silva, J.I. Pinto de Souza, Mater. Res. **2**, 279 (1999)
33. S.Y. Park, K. Kim, K.-H. Lim, B.J. Kim, E. Lee, J.H. Cho, Y.S. Kim, J. Mater. Chem. C **1**, 1383 (2013)
34. R.A. Rakkesh, S. Balakumar, Proc. Appl. Ceram. **8**(1), 7 (2014)
35. A.B. Djurišić, Y.H. Leung, Small **2**(8–9), 944 (2006)
36. S. Kumar, R. Thangavel, J. Sol-Gel. Sci. Technol. **67**, 50 (2013)
37. O. Lopatiuk-Tirpak, W.V. Schoenfeld, L. Chernyak, F.X. Xiu, J.L. Liu, A. Osinsky, P. Chow, Appl. Phys. Lett. **88**, 202110 (2006)
38. J. El Ghoul, M. Kraini, L. El Mir, J. Mater. Sci. Mater. Electron. **26**, 2555 (2015)
39. A. Wang, T. Chen, S. Lu, Z. Wu, Y. Li, H. Chen, Y. Wang, Nanoscale Res. Lett. **10**, 75 (2015)